Desalination and Water Treatment
www.deswater.com

doi: 10.5004/dwt.2017.20772

77 (2017) 194–205
May

Thermoeconomic analysis and optimization of a reverse osmosis desalination system driven by ocean thermal energy and solar energy

Qingxuan Sun, Jiangfeng Wang*, Pan Zhao, Yiping Dai

Institute of Turbomachinery, State Key Laboratory of Multiphase Flow in Power Engineering, School of Energy and Power Engineering, Xi'an Jiaotong University, Xi'an 710049, China, Tel./Fax: +86 029 82668704; emails: jfwang@mail.xjtu.edu.cn (J. Wang), sqx2234260@gmail.com (Q. Sun), pzhao@xjtu.edu.cn (P. Zhao), ypdai@xjtu.edu.cn (Y. Dai)

Received 24 July 2016; Accepted 11 April 2017

ABSTRACT

The utilization of solar and ocean energy for seawater desalination represents a significant prospect in solving energy crisis and water shortage. In this work, a new reverse osmosis desalination system based on ocean thermal energy conversion and solar energy utilization is proposed. The reverse osmosis system is driven by organic Rankine cycle, which obtains energy from ocean and solar energy, to produce freshwater. The mathematical model of the system is established and several indicators are employed to evaluate the system performance from the aspects of thermodynamics and thermoeconomic, including turbine shaft power, freshwater output, daily exergy efficiency, total water price and thermoeconomic unit cost. The effects of key thermodynamic parameters on the system performance and the system performance optimization with thermoeconomic unit cost and daily exergy efficiency as the objective functions based on the method of genetic algorithm are implemented. The results show that the turbine inlet pressure and the solar collection temperature have optimal values to reach the peak point of the system performance, while the increases of terminal temperature difference and pinch point temperature difference lead to a negative effect on the system performance. The exergy analysis shows that the main exergy losses occur in solar collector and heat exchangers.

Keywords: Solar energy; OTEC; Reverse osmosis; Thermoeconomic; Desalination

1. Introduction

Nowadays, fossil fuels have become an important restriction for social development and energy crisis has become a problem faced by all countries and humans. More and more attentions have been paid to renewable energy under the environmental deterioration, especially the solar energy, which has properties of huge amount and environment friendly. On the other hand, freshwater is another big problem that needs to be solved. Hence, the integrated system of solar energy and seawater desalination has been developed for years, in order to improve energy efficiency, reduce environmental pollution and alleviate the freshwater crisis.

1.1. Solar energy and reverse osmosis

Reverse osmosis (RO) is a potential method of seawater desalination, and some experts have conducted research on it for years. Reverse osmosis desalination technology exerts a high pressure, which is higher than the osmotic pressure, on one side of the membrane, to drive the water to another side, whereas the salt and other substance cannot pass through because of the permselectivity of membrane. The integrated system of reverse osmosis and solar power system has been quickly developed these years. Delgado-Torres and García-Rodríguez [1] and Ghermandi and Messalem [2] explored the feasibility of desalination system driven by solar powered organic Rankine cycle (ORC) and designed a new combined system of solar powered organic Rankine cycle and reverse osmosis desalination system. Delgado-Torres et al. [3]

* Corresponding author.

conducted preliminary thermodynamic analysis of a combined system of organic Rankine cycle, solar collector and reverse osmosis desalination. Based on the above research, Delgado-Torres and García-Rodríguez [4] also designed a two stages Rankine cycle desalination system. Kosmadakis et al. [5] proposed a new two stages organic Rankine cycle reverse osmosis desalination system and examined the feasibility by mathematical simulation. Kosmadakis et al. [6,7] also proposed some improvements of the proposed system, and then conducted a simulation and economic analysis to examine the performance improvement compared with single stage Rankine cycle system. Kosmadakis et al. [8] and Manolakos et al. [9] established a low temperature solar organic Rankine cycle powered reverse osmosis seawater desalination system and examined the performance of different working fluids. They compared 33 kinds of working fluids from thermal and environment aspects and found that R245fa was a good choice for solar organic Rankine cycle. Nafey et al. [10] established a solar organic Rankine cycle powered reverse osmosis desalination system based on different energy recovery ways and examined the performance from thermoeconomic analysis. Beside the theoretical research, some experimental studies were also conducted to validate the theoretical analysis. Manolakos et al. [11–13] also conducted some experiments of mid/low temperature organic Rankine cycle combined with reverse osmosis desalination system. El-Emam and Dincer [14] and Peñate and García-Rodríguez [15] had done some researches about thermoeconomic analysis of seawater reverse osmosis desalination plants.

It is obvious that the most of water desalination systems are setup in coastland where there are several kinds of energy sources, such as ocean thermal energy, tidal energy and wave energy. So it is convenient to integrate other form of energy with the present system to enhance the performance. Among them, the ocean thermal energy utilization is a promising technology which has been studied for years.

1.2. Ocean thermal energy conversion

The ocean thermal energy conversion (OTEC) system can perform the heat-work conversion utilizing temperature difference between warm surface seawater and cold deep seawater. The OTEC concept was conceived by D'Arsenoval first in 1881. Claude [16] and George and Paul [17] designed the first series of OTEC power system based on open and closed cycle, and the feasibility of OTEC from theoretical and experimental aspects had been examined by conducting experiments. Heydt [18] designed a 10 MW OTEC electricity generation system based on the analysis of thermal and economic performance. Nihous and Syed [19] put forward some suggestions to energy utilization and economic strategy in OTEC. Odum [20] made an energy analysis of a land-based OTEC system using emergy evaluation methods. Nihous [21] made a simple evaluation to global ocean thermal energy and pointed out that 5 TW stable ocean thermal energy could be utilized at most. Nihous [22] also made an evaluation on Atlantic Ocean thermal energy resources. Semmari et al. [23] designed a new Carnot cycle-based OTEC system with a hydraulic turbine to produce power.

It is evident that the low temperature difference between surface warm water and deep cool water leads to the low efficiency and high cost of OTEC system. Hence, integrating OTEC with other kinds of energy is developed to improve the efficiency, especially the solar energy.

1.3. Advantage of a combined system

Yamada et al. [24] proposed a solar-OTEC system using two kinds of energy utilizing methods including heating seawater directly and heating organic working fluid. Straatman and van Sark [25] designed a new combined system with OTEC and offshore solar energy collection system. Wang and Huang [26] conducted a dynamic-stability analysis of an offshore solar-concentrated OTEC system connected to an onshore power grid. Ahmadi et al. [27] conducted the energy and exergy analysis of an OTEC system driven by solar energy to produce hydrogen. Aydin et al. [28] conducted an analysis of a closed-cycle OTEC system with solar thermal collector integrated and analyzed two ways of utilizing solar energy.

Although some scholars conducted research on the integrated system of OTEC and solar energy to produce useful energy, little research has been conducted on the integrated system of OTEC and solar energy to produce freshwater using reverse osmosis desalination. In the present study, a reverse osmosis desalination system driven by ocean thermal energy and solar energy is developed. Daily exergy efficiency is defined to evaluate the performance of the system and some indicators are also employed to evaluate the thermoeconomic performance. Thermodynamic simulation and parametric analysis of the system are achieved based on a mathematical model, and a system performance optimization with thermoeconomic unit cost as the objective function is also conducted to obtain the best performance.

2. System description

The reverse osmosis desalination system in this study combines ocean thermal energy and solar energy together to produce freshwater. Fig. 1 illustrates a schematic diagram of the proposed reverse osmosis desalination system driven by ocean thermal energy and solar energy. This overall system consists of an energy collection subsystem, an organic Rankine cycle and an RO desalination subsystem.

The overall system obtains thermal energy mainly from energy collection subsystem. The thermal energy is converted to mechanical power by organic Rankine cycle, and the mechanical power drives RO desalination subsystem to produce freshwater. The energy collection subsystem consists of compound parabolic collector (CPC) and pump. CPC is selected as solar collector due to its high collection temperature, high efficiency and mature technique [29]. In organic Rankine cycle, R245fa is selected as the working fluid because of its good performance in thermodynamics and environment friendly. Pressure exchanger is employed in RO desalination subsystem owing to its better behavior among all kinds of energy recovery methods with a high efficiency of 92%–96% [30].

The warm surface seawater is pumped by water pump and heated in CPC by solar energy. Seawater with high temperature heats the organic working fluid in vapor generator and then discharges into sea. The heated organic fluid vapor is sent to turbine to produce mechanical works and turbine exhaust is delivered to a condenser to be condensed to liquid

by cold deep seawater. The turbine drives a high pressure pump to pump seawater to high pressure and the high pressure seawater is sent into reverse osmosis membrane unit, separated to two parts including the permeate freshwater and brine water. The permeate freshwater is the product, and the brine water which still has high pressure can be used in pressure exchanger to enhance the system performance.

The combined utilization of different energy can improve the system overall efficiency and enhance the freshwater output. Comparing with the air source condenser, the organic Rankine cycle condensed by cold seawater can have a higher efficiency and larger turbine shaft power due to the lower condensing temperature. And the ocean thermal energy can have a better performance due to a larger temperature difference. So, this combined system has a better performance and larger water output than single energy source system.

3. Mathematical model and performance criteria

The analyses of reverse osmosis system driven by OTEC and solar energy are required to be conducted from energy, exergy and thermoeconomic viewpoints. To simplify the theoretical model, some assumptions are made as follows:

- The system reaches a steady state.
- The pressure drops in CPC, vapor generator, condenser and the connection tubes are neglected.
- The turbine and pump, respectively, have a given isentropic efficiency.
- The stream at the condenser outlet is saturated liquid.

3.1. Thermodynamic model

CPC is a generally used solar collector which can absorb both beam and diffuse solar radiation [29]. The appropriate choice of CPC, which faces to the south in the northern hemisphere and has a suitable angle, can make the output temperature of working fluid reach higher. The main parameters of CPC are listed in Table 3.

The total effective flux absorbed S is:

$$S = \left[Ir_{be} R_{be} + \frac{Ir_{di}}{Cr} \right] \tau\rho\alpha \tag{1}$$

where $Ir_{be}R_{be}$ is the bean radiation flux accepted by CPC, and $\frac{Ir_{di}}{Cr}$ is the diffuse radiation flux accepted by collectors.

The useful heat gain rate Q_u can be calculated by the following equations:

$$Q_u = F_R WL \left[S - \frac{u_{lo}}{Cr} (T_{fi} - T_a) \right] \tag{2}$$

where

$$F_R = \frac{\dot{m}_{solar} c_p}{b u_{lo} L} \left\{ 1 - \exp\left[\frac{F' b u_{lo} L}{\dot{m}_{solar} c_p} \right] \right\} \tag{3}$$

and

$$\frac{1}{F'} = u_{lo} \left[\frac{1}{u_{lo}} + \frac{b}{N\pi D_i k} \right] \tag{4}$$

The mathematical model of solar energy collection is based on the research of Sen [29].

In the organic Rankine cycle, working fluid, i.e., R245fa, absorbs heat from warm water in vapor generator and is condensed by cold water in condenser. The T–s diagram of organic Rankine cycle is shown in Fig. 2.

The energy absorbed by R245fa from warm water in vapor generator is:

$$Q_{ge} = \dot{m}_{orc} (h_1 - h_5) \tag{5}$$

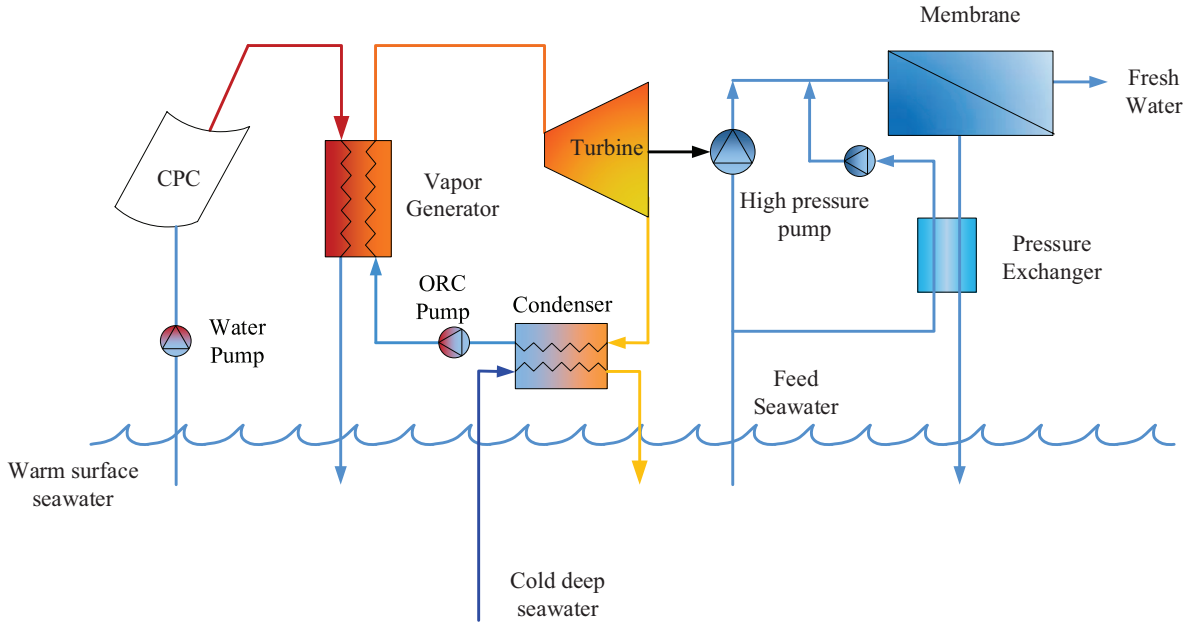

Fig. 1. Schematic diagram of the reverse osmosis desalination system driven by ocean thermal energy and solar energy.

The shaft power of ORC turbine is:

$$W_{tur} = m_{orc}(h_1 - h_2) \tag{6}$$

The isentropic efficiency of turbine can be expressed as:

$$\eta_{tur} = \frac{h_1 - h_2}{h_1 - h_{20}} \tag{7}$$

The works input by the pump is:

$$W_{pump} = \dot{m}_{ORC}(h_4 - h_3) \tag{8}$$

The isentropic efficiency of pump can be defined by:

$$\eta_{pump} = \frac{h_{40} - h_3}{h_4 - h_3} \tag{9}$$

The net mechanical power of ORC subsystem is:

$$W_{net} = W_{tur} - W_{pump} \tag{10}$$

The net energy efficiency of ORC subsystem can be calculated by:

$$\eta_{net} = \frac{W_{tur}}{Q_u} \tag{11}$$

The mathematical model of reverse osmosis is based on the research of El-Dessouky and Ettouney [31].

The mass flow rate and salt concentration balance in reverse osmosis are expressed as:

$$\dot{m}_f = \dot{m}_p + \dot{m}_b \tag{12}$$

$$X_f \dot{m}_f = X_p \dot{m}_p + X_b \dot{m}_b \tag{13}$$

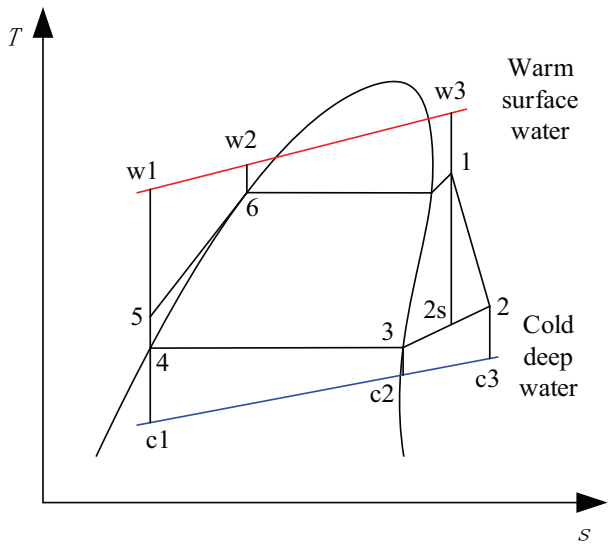

Fig. 2. *T*–*s* diagram of the organic Rankine cycle.

The mass flow rate of feedwater can be calculated as follow, which is influenced by mass flow rate of permeate water and recovery ratio RR, which is affected by salinity of the feedwater and the system design parameters, in this system the value of RR is given as 0.5:

$$m_f = \frac{m_p}{\mathrm{RR}} \tag{14}$$

The mass flow rate of permeate freshwater is calculated by:

$$\dot{m}_p = (\Delta p - \Delta\pi) K_w A_m \tag{15}$$

where Δp is water pressure difference, $\Delta\pi$ is osmotic pressure difference between feed side and brine side respectively, K_w is water permeability and A_m is membrane area.

The mass flow rate of feedwater output driven by the mechanical power W_{net} is estimated as:

$$m_f = \frac{\rho_f \eta_P W_{net}}{\Delta P} \tag{16}$$

where ΔP refers to the pressure difference across high pressure pump.

The water output varies across the period of 1 d because of the variation of solar radiation. Therefore, a modified water output indicator is proposed to determine the total water output of 1 d. The total freshwater output during a period of 1 d can be calculated as follow:

$$V_{day} = \int_{day} \frac{\dot{m}_f}{\rho_{water}} dt \tag{17}$$

3.2. Exergy model

Exergy is the maximum theoretical work obtainable from an overall system consisting of the system and the environment as the system comes into equilibrium with the environment [32]. Exergy analysis is usually conducted to assess the departure of the state of the system from that of the environment. In the present study, the exergy analysis only considers the physical exergy ignoring the other forms of exergy such as chemical exergy.

The physical exergy at a state point *i* can be defined as:

$$E_i = \dot{m}_i \left[\left(h_i - h_a \right) - T_a (s_i - s_a) \right] \tag{18}$$

The exergy received by CPCs is calculated by:

$$E_{solar} = A_{cpc} S \left[1 + \frac{1}{3} \left(\frac{T_a}{T_{solar}} \right)^4 - \frac{4}{3} \frac{T_a}{T_{solar}} \right] \tag{19}$$

where the A_{cpc} is the total area of CPC collectors, S is solar radiation absorbed and T_{solar} is the solar radiation temperature of 6,000 K [33].

The exergy balance of a single unit can be expressed as [34]:

$$\sum E_{input} - \sum E_{output} = I \tag{20}$$

The total exergy loss of an overall system is:

$$I_{sys} = \sum I \tag{21}$$

The exergy efficiency, also called second-law efficiency, is an important indicator for system performance evaluation, which can be expressed as:

$$\eta_{exergy} = \frac{W_{net}}{E_{solar}} \tag{22}$$

Based on the variation of solar radiation, it is necessary to modify the basic exergy efficiency to evaluate the system performance over a day. Therefore, daily exergy efficiency is defined as:

$$\eta_{exg} = \frac{W_{day}}{E_{day}} = \frac{\int W_{net}\mathrm{d}t}{\int E_{solar}\mathrm{d}t} \tag{23}$$

3.3. Thermoeconomic model

Thermoeconomic analysis is a useful and powerful method to evaluate system performance from the aspects of both thermodynamics and economics. In the present study, the thermoeconomic model of overall system consists of the energy collection subsystem and organic Rankine cycle as well as the RO desalination subsystem. The thermoeconomic indicator, namely thermoeconomic unit cost $c_{product}$ is employed based on the costs of equipment, exergy input and exergy output during the lifetime of the system.

Regarding the costs of each equipment in energy collection subsystem, organic Rankine cycle, and RO desalination subsystem, the investment and operating and maintenance costs are calculated in Tables 1 and 2. In Table 1, DCC refers to the direct capital cost, O&M refers to operating and maintenance cost, TCC refers to total capital cost and $Z^{IC\&OM}$ stands for hourly cost of investment, operating and maintenance. Due to the interest rate, which is considered as 5%, and exchange rate between dollar and Chinese Yuan, whose value is 6.6 when this paper is finished, the coefficients of cost calculation have been recalculated.

Considering the lifetime of the system, the amortization factor is adopted to reflect the influence of system run time. The amortization factor a is expressed in the following relation [34]:

$$a = \frac{i(1+i)^{LTp}}{(1+i)^{LTp-1}} \tag{24}$$

where i is the interest rate of 5%, LT_p is the plant lifetime of 20 years.

The total cost of the overall system is defined as:

$$TCC_{total} = TCC_{cpc} + TCC_{vg} + TCC_{tur} + TCC_{cond} + TCC_{pump} + TCC_{RO} \tag{25}$$

The hourly total cost including investment, operating and maintenance cost is another important indicator in economics, which reflects the hourly cost of the system and is given by:

$$Z_{total} = Z_{cpc} + Z_{vg} + Z_{tur} + Z_{cond} + Z_{pump} + Z_{RO} \tag{26}$$

The freshwater price is an important indicator to evaluate the system economic performance, which represents the unit price of freshwater. The total water price can be calculated as:

$$TWP = \frac{TCC_{total}}{V_{day} \cdot n \cdot PA} \tag{27}$$

where n refers to the days of a year.

Table 2
Cost of RO subsystem [31]

Membrane purchase cost (MPC, ¥)	60% × DCC_{ro}
Plant availability (PA)	0.9
Annual fixed charges (AFC, ¥/y)	A_f × DCC_{ro}
Electric cost (EC, ¥/m^3)	0.25
Annual membrane replacement cost (AMRC, ¥/y)	10% × MPC
Specific chemicals cost (SCC, ¥/m^3)	0.21
Annual chemicals cost (ACC, ¥/y)	SCC × PA × V_{day} × 365
Specific cost of operating labor (SCL, ¥/m^3)	0.03
Annual labor cost (ALC, ¥/y)	SCL × PA × V_{day} × 365
Total capital cost (TCC, ¥/y)	AFC + AMRC + ACC + ALC
Operating and maintenance costs ($O\&M_{ro}$, ¥)	0.02 × DCC_{ro}
Investment and O&M cost ($Z^{IC\&OM}$, ¥/h)	(TCC + A_f × $O\&M_{ro}$)/8,760

Table 1
Cost of each component in energy collection subsystem and ORC [35]

Components	DCC, ¥	O&M, ¥	TCC, ¥/y	$Z^{IC\&OM}$, ¥/h
CPC	1,960 × $(A_{cpc})^{0.95}$	15% × DCC_{cpc}	A_f × $(DCC + O\&M)_{cpc}$	TCC_{col}/8,760
Vapor generator	1,960 × $(A_{vg})^{0.8}$	25% × DCC_{vg}	A_f × $(DCC + O\&M)_{vg}$	TCC_{vg}/8,760
Turbine	61,130 × $(W_{tur})^{0.75}$	25% × DCC_{tur}	A_f × $(DCC + O\&M)_{tur}$	TCC_{tur}/8,760
Condenser	1,960 × $(A_{cond})^{0.75}$	25% × DCC_{cond}	A_f × $(DCC + O\&M)_{cond}$	TCC_{cond}/8,760
Pump	45,738 × $(W_{pump})^{0.47}$	25% × DCC_{pump}	A_f × $(DCC + O\&M)_{pump}$	TCC_{pump}/8,760

For a system, the thermoeconomic balance can be written as [36]:

$$\sum_{\text{out}} C = \sum_{\text{in}} C + Z^{\text{IC\&OM}} \tag{28}$$

where thermoeconomic cost C can be expressed as follow:

$$C_{i,o} = c_{i,o} E_{i,o} \tag{29}$$

$$C_w = c_w E_w \tag{30}$$

$$C_q = c_q E_q \tag{31}$$

where c refers to average cost per unit of exergy and the subscripts i, o, w and q refer to inlet, outlet, power and energy, respectively.

Based on the thermoeconomic fundamentals as presented in Eqs. (28)–(31), the thermoeconomic balance equations for each component can be calculated and integrated into one thermoeconomic balance equation of the overall system.

$$C_{\text{product}} = C_{\text{w-pump}} + Z_{\text{total}} \tag{32}$$

So the thermoeconomic indicator, thermoeconomic unit cost c_{product} can be calculated as:

$$c_{\text{product}} = \frac{c_{\text{w,cpc,pump}} E_{\text{w,cpc,pump}} + c_{\text{w,orc,pump}} E_{\text{w,orc,pump}} + c_{\text{w,ro,pump}} E_{\text{w,ro,pump}} + Z_{\text{total}}}{E_{\text{product}}} \tag{33}$$

where E_{product} is the exergy of the product stream from RO desalination system.

4. Results and discussion

The simulation of the overall system was carried out using a simulation program written by authors with Matlab. Thermodynamic properties of the working fluid were calculated by REFPROP 9.0 [37]. Sanya in China is selected as the case city and June 1st is chosen as the simulation date, and it is also assumed that the day is a typical sunny day that the system can experience a whole period of variation in the solar radiation. The flow chart of the simulation procedure is shown in Fig. 3.

4.1. Analysis of key parameters

A constant temperature of 293 K with the atmospheric pressure of 0.1 MPa is set as the reference state for energy and exergy calculation. The main parameters of the simulation are listed in Table 3.

Table 4 shows the elementary simulation results of the overall system based on the above parameters. The results can be found that the average turbine shaft power is 122.98 kW and the daily freshwater output reaches 990.56 m^3. The net energy efficiency of organic Rankine cycle is 6.69% while the daily exergy efficiency is 3.3%.

Fig. 4 indicates that the solar radiation and freshwater output during a day. It can be seen that the solar radiation begins on 6:00 and ends on 18:00 and it reaches its maximal value at noon. The variation of freshwater output is almost the same as solar radiation. But as we can see, in the first two and last 2 h, the freshwater output is zero because the solar radiation is not strong enough to support system running. So the system's operation time is between 8:00 and 16:00. We can get the daily freshwater output and average freshwater output in this operation period, shaft power, exergy and other variables are also calculated during this period. The following calculation and analysis is based on this system operation period.

Based on the above results, the key parameters, namely, turbine inlet pressure, solar collection temperature, condenser terminal temperature difference and pinch point temperature difference, are examined to evaluate their effects on the system performance from the perspectives of thermodynamics and thermoeconomic. One of the parameters is varied while the other three parameters kept constant and the value of each parameter is based on Table 3.

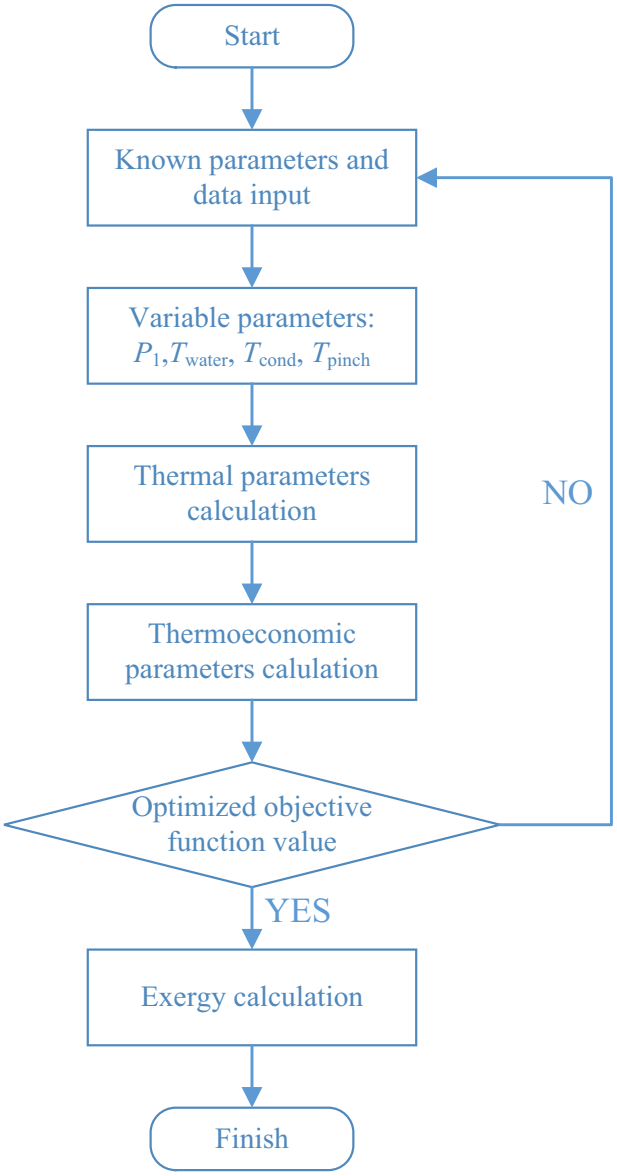

Fig. 3. Flow chart of the simulation procedure.

The effect of turbine inlet pressure on system performance is illustrated in Figs. 5 and 6 for thermodynamics and thermoeconomic. It can be seen that, with turbine inlet pressure increase, daily exergy efficiency, turbine shaft power and freshwater output increase at first and then decline. An increase in turbine inlet pressure leads to an increase in enthalpy difference across turbine, which causes the increase of shaft power. But when turbine inlet pressure rise, the mass flow rate of working fluid decrease. When the turbine inlet pressure is too high, the high enthalpy difference across turbine cannot make up the negative effect caused by decreasing mass flow rate of working fluid, hence, the system performances start to deteriorate. It can be found in Fig. 5 that the total water price and thermoeconomic unit cost reach the best performance when turbine inlet pressure reaches approximately 700 kPa. Since the hourly total cost is determined by

Table 3
Conditions of the simulation of the overall system

City	Sanya, China
Latitude	18°N
Ambient temperature, K	293
Ambient pressure, kPa	101
Warm surface water temperature, K	298
Cold deep water temperature, K	278
Concentration ratio of CPC	6.5
Area of single CPC, m	235
Number of CPC	42
Specific heat capacity of water, J/(kg·K)	4,200
Pinch point temperature difference, K	5
Condenser terminal temperature difference, K	7
Turbine isentropic efficiency, %	75
Pump isentropic efficiency, %	75
Turbine inlet pressure, kPa	700
Solar collection temperature, K	400
Salinity of seawater, kg/m^3	45
Salinity of brine water, kg/m^3	69
Salinity of permeate water, kg/m^3	0.145
Pressure of seawater, kPa	8,000
Pressure of brine water, kPa	7,800
Pressure of permeate water, kPa	101

Table 4
Elementary results of the simulation of the overall system

Average turbine shaft power, kW	122.98
Average mass flow rate of R245fa, kg/s	2.79
Daily shaft power, kWh	983.87
Daily freshwater output, m^3	990.56
Net energy efficiency, %	6.69
Daily exergy efficiency, %	3.3
RO membrane area, m^2	2,418
Vapor generator heat exchange area, m^2	815.44
Condenser heat exchange area, m^2	2,051.7
TPC, ¥/y	1.677×10^6
Z_{total}, ¥/h	83.93
TWP, ¥/m^3	4.32
$c_{product}$, ¥/GJ	106.07

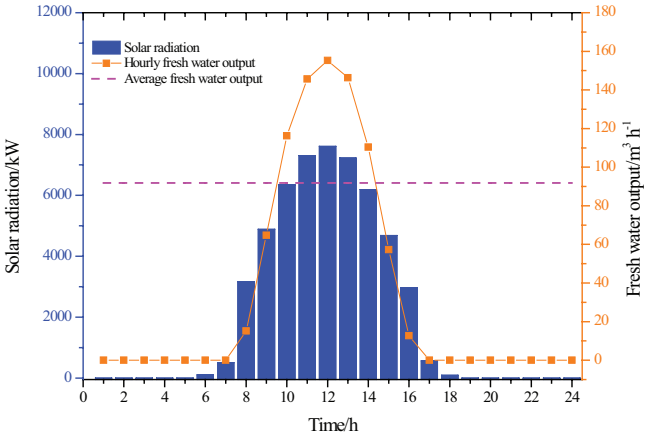

Fig. 4. Solar radiation and freshwater output varies during a day.

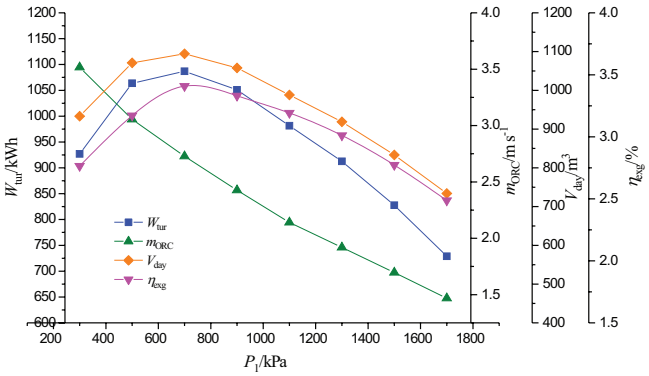

Fig. 5. Effect of turbine inlet pressure on thermodynamic performance.

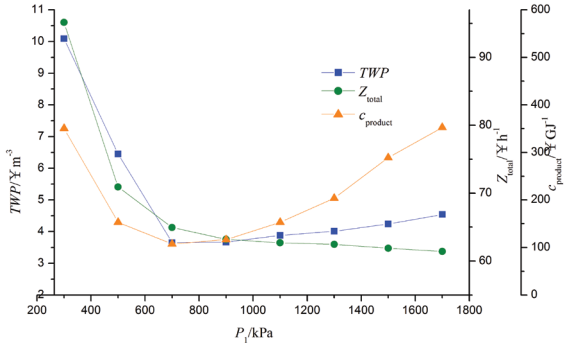

Fig. 6. Effect of turbine inlet pressure on thermoeconomic performance.

each equipment cost which decrease along with the decrease of mass flow rate of working fluid, so Z_{total} decrease with the increase of turbine inlet pressure. In a word, there exists an optimal turbine inlet pressure to achieve the best thermoeconomic performance.

Figs. 7 and 8 illustrate the effect of solar collection temperature on system performance. The change of solar collection temperature has an obvious effect on system performance. With the increase of solar collection temperature, both the turbine shaft power and the mass flow rate of working fluid increase because of the rise of energy gained from solar radiation. But when the solar collection temperature is too high, the increase of temperature brings a negative effect on system performance, because high temperature leads to low mass flow rates of water and working fluid in ORC. So the mass flow rate of working fluid in ORC increases at first and decreases when solar collection temperature is too high of 6,000 K. But it can be found that the daily exergy efficiency rises along with the increase of solar collection temperature because of the high turbine inlet temperature in ORC. Since the freshwater output and mass flow rate of working fluid in ORC have optimal values, solar collection temperature also has a peak point for system economic and thermoeconomic performance. Due to the variation of mass flow rate of working fluid in ORC, Z_{total} increases at first and then decreases when solar collection temperature is too high. The total water price and thermoeconomic unit cost also decrease at first and then increase. Therefore, solar collection temperature has a peak point for system performance, in this case it is approximate 400 K.

The influence of condenser terminal temperature difference on system performance is shown in Figs. 9 and 10. It is obvious that the increase of terminal temperature difference has a negative effect on system performance. The increase of terminal temperature difference leads to the increase of turbine back pressure, which reduces the daily exergy efficiency, turbine shaft power and freshwater output. At the same time, the unchanged mass flow rate of working fluid in ORC and the decrease of freshwater output lead to the slight drop of thermoeconomic performance. The cost per hour keeps steady, the total water price and thermoeconomic unit cost increase slightly due to the decrease of water output.

The effect of pinch point temperature difference is shown in Figs. 11 and 12. It is evident that the increase of pinch point temperature difference brings a negative effect on system performance. The increase of pinch point temperature leads to the decrease of energy gained from vapor generator, so the turbine shaft power, freshwater output, daily exergy efficiency and mass flow rate of working fluid decrease in the same time. And from Fig. 11 it can be found that, system economic and thermoeconomic performance are also getting bad when pinch point temperature increase. In a word, the increase of pinch point temperature difference leads a negative effect on system performance.

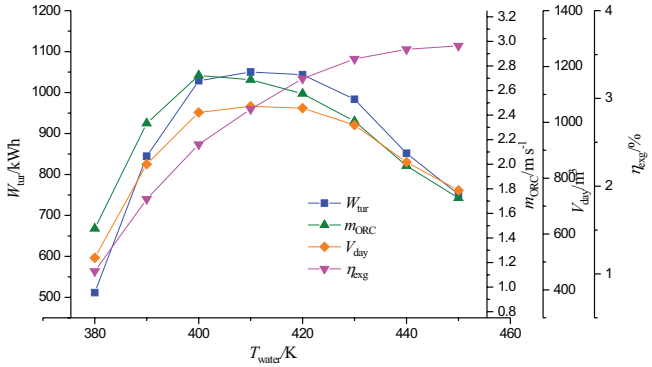

Fig. 7. Effect of solar collection temperature on thermodynamic performance.

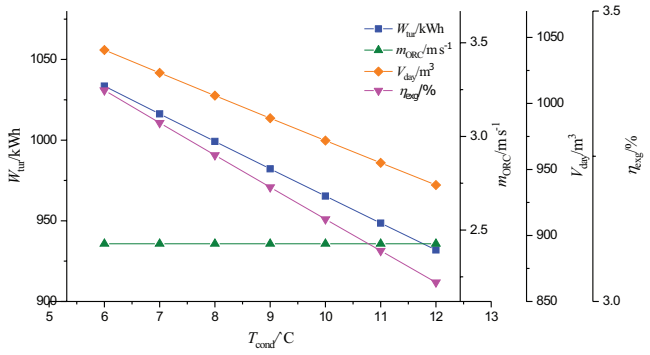

Fig. 9. Effect of terminal temperature difference on thermodynamic performance.

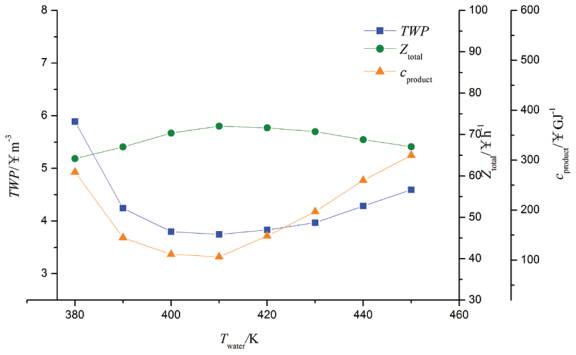

Fig. 8. Effect of solar collection temperature on thermoeconomic performance.

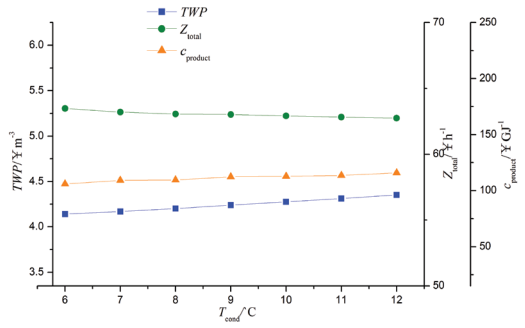

Fig. 10. Effect of terminal temperature difference on thermoeconomic performance.

4.2. Multi-objective optimization result based on thermoeconomic

According to previous analysis of the effects of these key parameters on the performance of the system, it can be found that the key parameters have different effects on the system under different conditions. Since the performance of the proposed system is not governed by one parameter but the combination of the several key parameters, it is essential to find the optimized group of parameters which vary over reasonable ranges, in order to achieve the best performance of the system. This paper will conduct a multi-objective optimization for the desalination system.

A multi-objective optimization searches the solution that meets demand of different performance indicators simultaneously. The multi-objective optimization process can be described as:

$$\min F(x) = [f_1(x), f_2(x), \ldots, f_n(x)]^T \tag{34}$$

$$x_{k,\min} \le x_k \le x_{k,\max} \tag{35}$$

where x means the vector of decision parameters, $F(x)$ denotes the vector of objective functions, $x_{k,\min}$ and $x_{k,\max}$ are the bottom and top limit of the decision parameters.

Genetic algorithm (GA) [38] is an evolutionary algorithm inspired by evolutionary biology that uses some techniques such as selection, crossover and mutation to search for the best solution. GA, as a powerful and broadly applicable stochastic search and optimization technique, is perhaps the most widely known types of evolutionary computation method today [39]. Non-dominated sorting genetic algorithm II (NSGA-II) as a multi-objective optimization method of GA is employed to achieve the multi-objective optimization of the reverse osmosis desalination system driven by ocean thermal energy and solar energy. The control parameters of NSGA-II for the reverse osmosis desalination system driven by ocean thermal energy and solar energy are listed in Table 5.

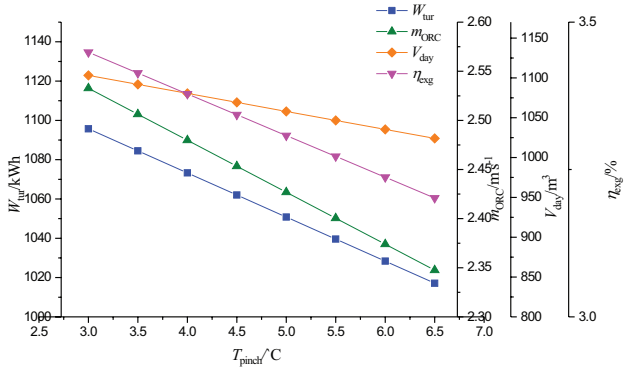

Fig. 11. Effect of pinch point temperature difference on thermodynamic performance.

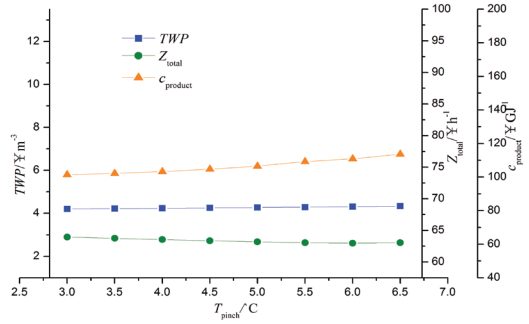

Fig. 12. Effect of pinch point temperature difference on thermoeconomic performance.

In this study, we select the thermoeconomic unit cost and the daily exergy efficiency as two objective functions. Four key thermodynamic parameters, namely turbine inlet pressure, terminal temperature difference, pinch point temperature difference and solar collection temperature are chosen as the decision parameters due to their significant effects on the system performance. The limit of each decision parameters is based on the above analysis. The ranges of the decision parameters are listed in Table 6.

Fig. 13 shows the optimal solution of thermodynamic parameters for the system performance by multi-objective optimization. It can be seen that increasing the thermoeconomic unit cost causes an increase in the daily exergy efficiency. Table 7 lists the optimal values of the two performance indicators and corresponding decision parameters. The final solution among the optimal values could be selected and the selection process is carried out according to engineering experience and the importance of each objective.

Since the exergy also varies in a period of 1 d, the exergy analysis has been based on the daily exergy efficiency. As illustrated in Fig. 14, due to the high temperature of the solar radiation and the temperature difference between the solar collector and inlet water, the solar collector contributes to the largest part of exergy loss. The second largest exergy loss

Table 5
Control parameters of NSGA-II

Control parameters	Value
Population size	90
Maximum generations	200
Crossover probability	0.8
Mutation probability	0.05
Selection process	Tournament

Table 6
The ranges of the decision parameters

Decision parameters	Lower limit	Upper limit
Turbine inlet pressure, kPa	200	1,200
Terminal temperature difference, K	5	15
Pinch point temperature difference, K	5	8
Solar collection temperature, K	370	450

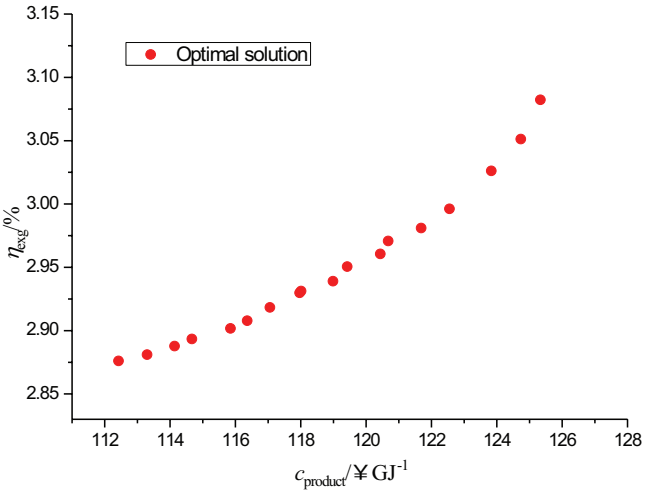

Fig. 13. Optimal solution for the net energy efficiency vs. the thermoeconomic unit cost.

Table 7
Optimal values and corresponding decision parameters

$c_{product}$ (¥/GJ)	η_{exg} (%)	P_1 (kPa)	T_{water} (K)	T_{cond} (K)	T_{pinch} (K)
113.30	2.88	712.37	405.25	5.24	5.13
117.06	2.88	721.41	410.53	5.12	5.26
114.67	2.89	686.29	409.38	5.34	5.17
115.85	2.89	695.48	406.82	5.21	5.48
123.83	2.90	705.64	416.28	5.38	5.24
125.33	2.91	714.24	403.56	5.19	5.36
117.96	2.92	703.48	412.15	5.24	5.17
118.01	2.93	683.51	405.89	5.42	5.25
112.42	2.93	694.63	411.15	5.16	5.45
119.42	2.94	686.58	405.68	5.37	5.31
120.43	2.95	708.45	406.74	5.14	5.26
120.68	2.96	714.24	408.67	5.34	5.19
121.69	2.97	698.53	402.68	5.67	5.24
122.55	2.98	701.62	409.17	5.27	5.34
118.99	2.99	716.48	401.96	5.21	5.16
124.73	3.02	690.45	406.28	5.38	5.18
116.36	3.05	703.61	403.54	5.34	5.27
114.14	3.08	684.48	407.32	5.26	5.30

occurred among equipment is in vapor generator, and the exergy loss in condenser is also significant. It can be indicated that the major exergy loss in ORC generally occurs in the heat exchangers, which may be caused by the temperature difference during the heat exchange process. But the temperature difference during vapor generator is much larger than temperature difference during condenser. So, some measures could be taken on the heat exchangers reduce the exergy losses, such as employing the optimization design method.

5. Conclusion

A desalination system based on ocean thermal energy and solar energy is investigated based on the thermoeconomic analysis in this work. The influences of some key parameters

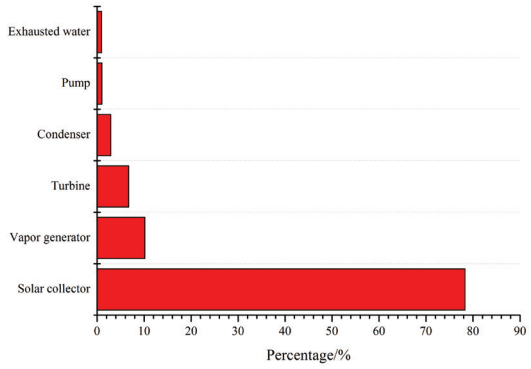

Fig. 14. Exergy loss distribution in system.

on the system performance are examined, the optimal values of these parameters are obtained via GA optimization, and the exergy analysis is conducted. The main conclusions drawn from the study are listed as follows:

- A reverse osmosis desalination system based on the OTEC and solar energy utilization is proposed. The ocean thermal energy and solar energy are combined to improve the energy utilization efficiency.
- The turbine inlet pressure has an optimal value to reach the best system performance. There is an optimal solar collection temperature that yields the maximum water output of the RO desalination subsystem. In addition, the increase of condenser terminal temperature difference and pinch point temperature brings a negative influence on the system performance.
- A multi-objective optimization is conducted and the result shows that an increase in the thermoeconomic unit cost would increase the net energy efficiency. The optimal design solution and their corresponding decision variables are listed and needed to be selected by a process of decision-making.
- The exergy analysis based on the optimal parameters shows that the main exergy loss of overall system mainly exists in solar collector, following with the heat exchangers, especially vapor generator.

Acknowledgment

The authors gratefully acknowledge the financial support by the National Natural Science Foundation of China (Grant No. 51476121) and the K. C. Wong Education Foundation.

Symbols

A	—	Area, m^2
a	—	Amortization factor
b	—	Width of absorber, m
Cr	—	Concentration ratio of CPC
C	—	Cost, ¥
c	—	Thermoeconomic unit cost, ¥/GJ
c_p	—	Specific heat, kJ/kg K
D	—	Diameter, m

E	—	Exergy, kW
F'	—	Collector efficiency factor
F_R	—	Heat removal factor
h	—	Specific enthalpy, kJ/kg
Ir	—	Hourly radiation, W/m^2
I	—	Exergy loss rate, kW
i	—	Interest rate
k	—	Heat transferring coefficient, W/m^2 K
K_w	—	Water permeability coefficient, m^3/m^2 s kPa
L	—	Length, m
$\dot{m}$	—	Mass flow rate, kg/s
N	—	Number of tubes
p	—	Pressure, MPa
Q	—	Heat load, kW
R	—	Tilt factor for radiation
RR	—	Recovery ratio
S	—	Incident solar flux, W/m^2
s	—	Specific entropy, kJ/kg K
T	—	Temperature, K
u	—	Loss coefficient, W/m^2 K
U	—	Heat transfer coefficient, W/m^2 K
V	—	Volume, m^3
W	—	Power, kW
x	—	Quality
X	—	Salinity, kg/m^3

Greek

α	—	Absorptivity of the absorber surface
η	—	Efficiency
π	—	Osmotic pressure, kPa
ρ	—	Reflectivity of the concentrator surface; density, kg/m^3
τ	—	Transmissivity of the cover

Subscripts

a	—	Ambient
b	—	Brine water flow
be	—	Beam
cpc	—	Compound parabolic collector
di	—	Diffuse
day	—	A period of a day
exg	—	Exergy
f	—	Feedwater flow
ge	—	Vapor generator
lo	—	Loss
load	—	Load
net	—	Net value
orc	—	Organic Rankine cycle
p	—	Permeate water flow
pump	—	Pump
sys	—	System
tur	—	Turbine
u	—	Useful

References

[1] A.M. Delgado-Torres, L. García-Rodríguez, Status of solar thermal-driven reverse osmosis desalination, Desalination, 216 (2007) 242–251.

[2] A. Ghermandi, R. Messalem, Solar-driven desalination with reverse osmosis: the state of the art, Desal. Wat. Treat., 7 (2009) 285–296.

[3] A.M. Delgado-Torres, L. García-Rodríguez, V.J. Romero-Ternero, Preliminary design of a solar thermal-powered seawater reverse osmosis system, Desalination, 216 (2007) 292–305.

[4] A.M. Delgado-Torres, L. García-Rodríguez, Double cascade organic Rankine cycle for solar-driven reverse osmosis desalination, Desalination, 216 (2007) 306–313.

[5] G. Kosmadakis, D. Manolakos, S. Kyritsis, G. Papadakis, Simulation of an autonomous, two-stage solar organic Rankine cycle system for reverse osmosis desalination, Desal. Wat. Treat., 1 (2009) 114–127.

[6] G. Kosmadakis, D. Manolakos, S. Kyritsis, G. Papadakis, Economic assessment of a two-stage solar organic Rankine cycle for reverse osmosis desalination, Renew. Energy, 34 (2009) 1579–1586.

[7] G. Kosmadakis, D. Manolakos, S. Kyritsis, G. Papadakis, Design of a two stage Organic Rankine Cycle system for reverse osmosis desalination supplied from a steady thermal source, Desalination, 250 (2010) 323–328.

[8] G. Kosmadakis, D. Manolakos, S. Kyritsis, G. Papadakis, Comparative thermodynamic study of refrigerants to select the best for use in the high-temperature stage of a two-stage organic Rankine cycle for RO desalination, Desalination, 243 (2009) 74–94.

[9] D. Manolakos, G. Kosmadakis, S. Kyritsis, G. Papadakis, Identification of behaviour and evaluation of performance of small scale, low-temperature Organic Rankine Cycle system coupled with a RO desalination unit, Energy, 34 (2009) 767–774.

[10] A.S. Nafey, M.A. Sharaf, L. García-Rodríguez, Thermoeconomic analysis of a combined solar organic Rankine cycle-reverse osmosis desalination process with different energy recovery configurations, Desalination, 261 (2010) 138–147.

[11] D. Manolakos, G. Kosmadakis, S. Kyritsis, G. Papadakis, On site experimental evaluation of a low-temperature solar organic Rankine cycle system for RO desalination, Sol. Energy, 83 (2009) 646–656.

[12] D. Manolakos, G. Papadakis, S. Kyritsis, K. Bouzianas, Experimental evaluation of an autonomous low-temperature solar Rankine cycle system for reverse osmosis desalination, Desalination, 203 (2007) 366–374.

[13] D. Manolakos, G. Kosmadakis, S. Kyritsis, G. Papadakis, Identification of behaviour and evaluation of performance of small scale, low-temperature Organic Rankine Cycle system coupled with a RO desalination unit, Energy, 34 (2009) 767–774.

[14] R.S. El-Emam, I. Dincer, Thermodynamic and thermoeconomic analyses of seawater reverse osmosis desalination plant with energy recovery, Energy, 64 (2014) 154–163.

[15] B. Peñate, L. García-Rodríguez, Energy optimisation of existing SWRO (seawater reverse osmosis) plants with ERT (energy recovery turbines): technical and thermoeconomic assessment, Energy, 36 (2011) 613–626.

[16] G. Claude, Power from the tropical seas, Mech. Eng., 52 (1930) 1039–1044.

[17] C. George, B. Paul, Method and Apparatus for Obtaining Power from Sea Water, U.S. Patent 2,006,985, 1935.

[18] G.T. Heydt, An assessment of ocean thermal energy conversion as an advanced electric generation methodology, Proc. IEEE, 81 (1993) 409–418.

[19] G.C. Nihous, M.A. Syed, A financing strategy for small OTEC plants, Energy Convers. Manage., 38 (1997) 201–211.

[20] H.T. Odum, Emergy evaluation of an OTEC electrical power system, Energy, 25 (2000) 389–393.

[21] G.C. Nihous, A preliminary assessment of ocean thermal energy conversion resources, J. Energy Res. Technol., 129 (2007) 10–17.

[22] G.C. Nihous, An estimate of Atlantic Ocean thermal energy conversion (OTEC) resources, Ocean Eng., 34 (2007) 2210–2221.

[23] H. Semmari, D. Stitou, S. Mauran, A novel Carnot-based cycle for ocean thermal energy conversion, Energy, 43 (2012) 361–375.

[24] N. Yamada, A. Hoshi, Y. Ikegami, Performance simulation of solar-boosted ocean thermal energy conversion plant, Renew. Energy, 34 (2009) 1752–1758.

[25] P.J.T. Straatman, W.G. van Sark, A new hybrid ocean thermal energy conversion–offshore solar pond (OTEC–OSP) design: a cost optimization approach, Sol. Energy, 82 (2008) 520–527.
[26] L. Wang, C.B. Huang, Dynamic stability analysis of a grid-connected solar-concentrated ocean thermal energy conversion system, IEEE Trans. Sustain. Energy, 1 (2010) 10–18.
[27] P. Ahmadi, I. Dincer, M.A. Rosen, Energy and exergy analyses of hydrogen production via solar-boosted ocean thermal energy conversion and PEM electrolysis, Int. J. Hydrogen Energy, 38 (2013) 1795–1805.
[28] H. Aydin, H.S. Lee, H.J. Kim, Off-design performance analysis of a closed-cycle ocean thermal energy conversion system with solar thermal preheating and superheating, Renew. Energy, 72 (2014) 154–163.
[29] Z. Sen, Solar Energy Fundamentals and Modeling Techniques: Atmosphere, Environment, Climate Change and Renewable Energy, Springer Science & Business Media, Turkey, 2008.
[30] M. Wilf, C. Bartels, Optimization of seawater RO systems design, Desalination, 173 (2005) 1–12.
[31] H.T. El-Dessouky, H.M. Ettouney, Fundamentals of Salt Water Desalination, Elsevier, Netherlands, 2002.
[32] F.P. Incropera, A.S. Lavine, D.P. DeWitt, Fundamentals of Heat and Mass Transfer, John Wiley & Sons, USA, 2011.
[33] A. Malek, M.N.A. Hawlader, J.C. Ho, Design and economics of RO seawater desalination, Desalination, 105 (1996) 245–261.
[34] N. Lior, N. Zhang, Energy, exergy, and second law performance criteria, Energy, 32 (2007) 281–296.
[35] N.G. Voros, C.T. Kiranoudis, Z.B. Maroulis, Solar energy exploitation for reverse osmosis desalination plants, Desalination, 115 (1998) 83–101.
[36] A. Bejan, G. Tsatsaronis, M. Moran, Handbook of Thermal Design and Optimization, Wiley, New York, 1996.
[37] NIST Standard Reference Database 23, NIST Thermodynamic and Transport Properties of Refrigerants and Refrigerant Mixtures REFPROP, Version 8.0, 2007.
[38] J. Holland, Adaptation in Nature and Artificial Systems: An Introductory Analysis with Applications to Biology, Control and Artificial Intelligence, MIT Press, Massachusetts, 1992.
[39] M. Gen, R. Cheng, Genetic Algorithms and Engineering Optimization, John Wiley & Sons, USA, 2000.